PROCEEDINGS, 51st Workshop on Geothermal Reservoir Engineering
Stanford University, Stanford, California, February 9-11, 2026
SGP-TR-230

Radial Closed-Loop Geothermal Architectures for Phased Scaling: Thermal Performance Study

Samuel Tellier

Seattle, WA

sam@tellierdynamics.com

Keywords: Closed-Loop Geothermal, Advanced Geothermal Systems, AGS, Multilateral Well Systems, Thermosiphon, Hub-and-Spoke Architecture, Phased Scaling

Next-generation geothermal systems are advancing along two primary pathways: Enhanced Geothermal Systems (EGS) which create convective reservoirs via hydraulic fracturing, and Advanced Geothermal Systems (AGS), which extract heat via conduction through closed loops. While EGS offers high energy yields, it carries risks of induced seismicity and geological uncertainty. Conversely, conduction-based closed-loop systems mitigate seismicity, but face challenges related to thermal drawdown (short-circuiting) between proximal laterals and complex well-to-well interceptions. This paper introduces and evaluates the Telluric Radial System (TRS), a hub-and-spoke topology designed to synthesize the massive reservoir contact area of EGS with the low environmental risk of conductive systems. The architecture consists of a large-diameter, insulated central injection hub feeding a distributed network of single-layer, radially oriented production satellites. This configuration is hypothesized to offer superior geometric efficiency by eliminating the vertical thermal interference inherent in stacked parallel loop designs and accessing a larger volume of fresh rock, while consolidating well interception by targeting a stationary vertical hub. Furthermore, the design enables a phased scaling development model, allowing individual satellite radiators to be commissioned sequentially to stage risk and capital deployment. This study presents the conceptual framework and a comparative thermal performance analysis using 3D finite element modeling in OpenGeoSys utilizing parameters modeling the Malm Carbonate formation in Geretsried, Germany. Simulations were normalized for total drilling length to ensure an accurate comparison between radiator topologies. Results demonstrate that the single-layer TRS radiator maintains outlet temperatures 2°C to 5°C higher than equivalent multi-lateral stacked designs over a 30-year operational life, confirming that radial fanning effectively mitigates far-field thermal drawdown despite localized convergence at the hub. The model is further used to explore the system's sensitivity to key design parameters, including radial well spacing and the thermal resistance of the injector's insulation. This work provides a foundational assessment of the TRS as a pathway for developing scalable and dispatchable geothermal assets.

1. INTRODUCTION

The scaling of geothermal energy is currently constrained by the rarity of high-permeability hydrothermal reservoirs. Two primary solutions have emerged: Enhanced Geothermal Systems (EGS) (Tester et al. 2006), which create permeability via stimulation, and Advanced Geothermal Systems (AGS) or "Closed-Loop" systems, which rely on conductive heat extraction. While EGS offers high energy yields, it carries risks of induced seismicity and groundwater contamination. Conversely, closed-loop systems eliminate risks of induced seismicity, but require significantly higher drilling costs to install immense subsurface radiators, or rare geological conditions where simpler U-loop designs can leverage convective heat transfer through groundwater reservoirs. Existing closed-loop designs often employ "radiator" topologies with proximal parallel laterals going out-and-back (Beckers and Johnston, 2022) to enable drilling from a single pad. As heat is extracted by deeper laterals, the rock volume cools, thermally "shadowing" the laterals above.

The Telluric Radial System (TRS) is a closed-loop geothermal architecture designed to address these geometric inefficiencies while targeting the widely prevalent geological conditions. The TRS utilizes a hub-and-spoke topology where a central injection well feeds a network of radially distributed production wells. This study evaluates the TRS thermal performance using 3D finite element modeling with OpenGeoSys (Bilke et al. 2019) against a benchmark stacked-loop design. While intersecting nodes on a distant vertical hub multiple times presents significant guidance engineering challenges, this study focuses on highlighting the thermodynamic potential of the resulting geometry.

2. SYSTEM ARCHITECTURE

The TRS design comprises four major subsystems: the Central Injection Hub, Downhole Isolation Nodes, the Lateral Array, and the Satellite Outflow Wells, and utilizes a five-phase construction sequence.

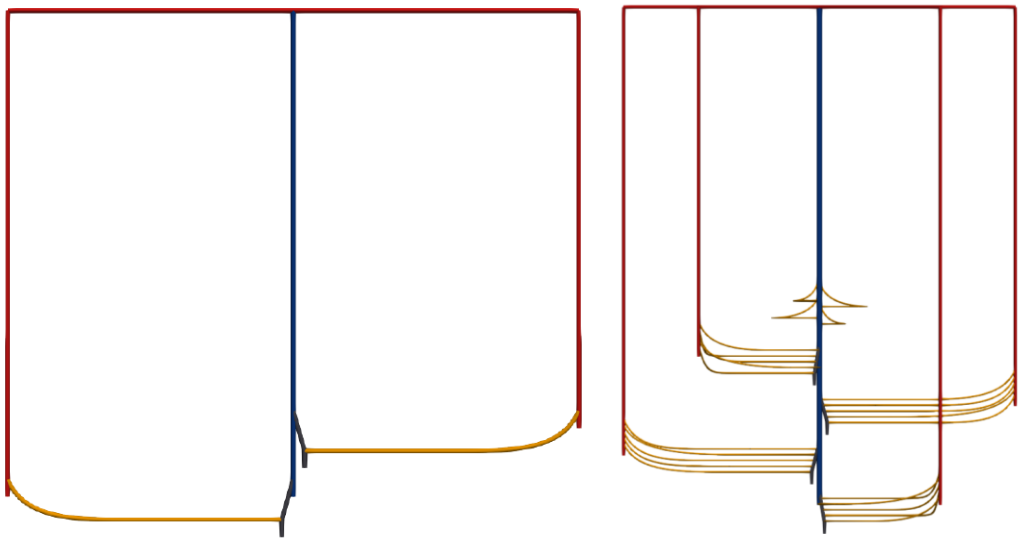

Figure 1: Two conceptual diagrams of the closed-loop "Telluric Radial System", depicting example configurations of blue central injector wells, black downhole isolation nodes extending down, yellow laterals, and red outflow and surface return pipes.

2.1 System Design

2.1.1 The Central Injection Hub

The primary vertical conduit utilizes a Telescoping Monobore design. The upper section features an expanded internal diameter to minimize fluid velocity and friction losses, tapering in the deep section to reduce drilling hook-load. The column is equipped with Vacuum Insulated Tubing (VIT) from surface down to the top of the reservoir interval to preserve the density of the cold injection fluid driving the thermosiphon effect. At the reservoir depth, the completion switches to standard production casing equipped with Pre-Milled Windows. These reinforced casing exits must be spaced and oriented to facilitate the installation and orientation of the Downhole Isolation Nodes while maintaining structural integrity of the well.

2.1.2 Downhole Isolation Nodes

A critical economic constraint of monolithic loop systems is the high upfront capital expenditure with multi-year deployment times before the first watt is generated. The TRS addresses this via "Live-Expansion." The reservoir interval contains an array of Downhole Isolation Nodes (Figure 1). These nodes function as multilateral junctions that provide:

1. **Drilling Safety:** A dual-barrier mechanism allowing new satellite laterals to be drilled and connected via the isolation nodes, minimizing system downtime.

2. **Hydraulic Isolation:** To facilitate live-well intervention with no downtime, the junction must provide pressure integrity equivalent to TAML Level 5 (Schlumberger 2023), ensuring mechanical and hydraulic isolation from the central injector.

3. **Flow Control:** Each node integrates a throttling mechanism to enable independent flow rate settings for each lateral, allowing mass flow to be equalized across the array despite varying lateral lengths, depths, and hydrostatic pressures.

4. **Intersection Geometry:** The node must provide sufficient axial length and internal clearance to accommodate the lateral intersection. A tail consisting of a liner with magnetic signatures can guide intersections gradually from close-range, and an under-reamed section can provide a larger surface area for intersecting laterals to land.

2.1.3 The Lateral Array (Heat Exchanger)

The subsurface heat exchanger consists of multiple linear horizontal conduits radiating from the central hub to the peripheral outflow wells. The laterals can be formation sealed (Toews et al. 2020) utilizing high-thermal-conductivity sealants or equipped with a liner where required. This creates a pressure-tight conduit for the working fluid while minimizing thermal resistance at the rock-bore interface. The design allows for variable horizontal and vertical offsets between laterals, enabling the optimization of conduction sweep efficiency across the reservoir volume.

2.1.4 The Outflow Network (Satellite Wells)

Thermal energy is transported to the surface via four vertical satellite wells located at the distal ends of the laterals. The entire production string is equipped with VIT to minimize heat loss during ascent, maintaining the low density of the hot column required for thermosiphon buoyancy. At the surface, pipes transport fluid to the central plant for power generation and form a distributed heating grid for direct-use thermal applications (e.g., district heating) before reinjection.

2.2 Construction Methodology & Phased Scaling

The construction and deployment of the TRS architecture follows a five-stage sequence: establishment of the central hub (Phase 1), operational readiness (Phase 2), modular expansion via live-well interception (Phase 3), loop activation (Phase 4), and steady-state dynamic management (Phase 5).

2.2.1 Base Infrastructure Deployment

Construction begins with the establishment of the central "Hub" to serve as the backbone for the system. The central injection well is drilled to total depth, and the production casing is set and completed. TAML level 5 intersections are installed for the Downhole Isolation Nodes, which are pressure tested incrementally to verify the mechanical integrity of nodes and seals against the casing. Nodal valves are set to their initially desired values, establishing the baseline configuration for the operational readiness phase.

2.2.2 Operational Readiness & Active Monitoring

Following the completion of the central hub, the system enters a state of active readiness while awaiting lateral connection. Any variable throttling valves are regularly actuated through their range of motion, reducing risk of mechanical seizure and ensuring continuous functionality of the flow-control hardware. An operator maintains active monitoring of the wellbore annulus and nodal interfaces. Continuous pressure diagnostics are utilized to detect potential leaks in the casing or isolation nodes, ensuring the double-barrier safety envelope remains intact prior to any drilling interception.

2.2.3 Live Modular Expansion

Once the base infrastructure is validated, the lateral heat exchangers are brought online progressively. This phase utilizes a hybrid magnetic ranging strategy to safely navigate the drilling assembly into the pre-installed nodes of the active injector. Drilling operations commence at the distant outflow pads, driving the lateral sections inbound towards the central hub utilizing MWD (Measurement While Drilling) technology. This provides inertial navigation to maintain the planned trajectory before the assembly is within range of active magnetic ranging sources (Halliburton, 2024, Scientific Drilling 2024) from the central injector. The circulating cold fluid protects active magnetic ranging sources from the geothermal gradient, providing a strong, active signal for the drill bit to track. As the drill approaches the tail of the node, it gets within range of the passive magnetic signatures of the node to guide a gradual intersection. Prior to intersection with a live well, the integrity of the Downhole Isolation Node must be verified with a pressure test to ensure the barrier system is fully competent. Once alignment and barrier integrity are confirmed, the drilling assembly intersects the node. The lateral is then sealed to the node, either chemically or with a liner.

2.2.4 Node Activation

Activation procedures are initiated only after all laterals associated with a specific Outflow Well have been successfully connected, sealed, and pressure tested. With the loop fully integrated, the Dual-Barrier Safety Mechanism is retrieved, dissolved, or discarded in a sump to clear the flow path. Surface circulation pumps are utilized as needed to prime the new lateral loop, overcoming initial static friction and establishing the density differential required to sustain passive thermosiphon flow.

2.2.5 Continuous Operation & Dynamic Control

Following activation, the system enters a steady-state operational mode governed by real-time telemetry and active reservoir management. The central injection flow rate is dynamically modulated based on the aggregated demand communicated by the satellite outflow wells. As the thermal resource matures, the throttling valves can be adjusted to re-balance flow across the array as needed, increasing residence time in cooler laterals or prioritizing flow to higher-temperature zones to maintain the target output temperature. Outflow temperatures, pressures, and flow rates are continuously monitored at each satellite and communicated to the central control. In the event of a casing breach or component failure, individual laterals or entire outflow sectors can be isolated.

3. METHODOLOGY

We employ numerical simulations to investigate the thermal performance of distinct subsurface radiator geometries over a 30-year operational horizon. The analysis utilizes OpenGeoSys (OGS), an open-source finite element simulator, to model the coupled thermal-hydraulic processes. The simulation adopts the HEAT_TRANSPORT_BHE process with 1P (single U-tube/pipe) elements. This formulation discretizes the wellbore as 1D finite elements coupled to the 3D finite element mesh of the subsurface. The governing equations solve for convective heat transport within the pipe network with conductive heat transfer in the surrounding porous medium, utilizing a heat transfer coefficient to mediate the thermal flux at the borehole interface. This approach captures the transient thermal interaction at the borehole wall while reducing the dimensionality of the fluid flow problem compared to a full 3D CFD discretization.

3.1 Simulation Environment & Parameters

The simulation domain is defined as a block model with homogeneous material properties (conductivity, density, porosity) to isolate geometric effects from lithological heterogeneity. The domain is initialized with a vertical temperature gradient to reflect the in-situ thermal stress regime. The simulation input parameters (Table 1) were selected to benchmark the TRS against a state-of-the-art reference radiator geometry, modeled on specifications from the commercial closed-loop demonstrator in Geretsried, Germany (adapted from Kelly et al. 2022; Richter 2024). The rock properties are representative of the Malm Carbonate formation, and the baseline stacked-loop geometry is derived from publicly available design data (Kelly et al. 2022). The circulated fluid is assumed to be based on water. Constant density was employed in the subsurface FEM to reduce computational cost during long-term transient heat transport solving, while the

precise variable-density hydraulic coupled model was applied post-process to capture the buoyancy effects in the vertical columns where pressure differentials are most critical.

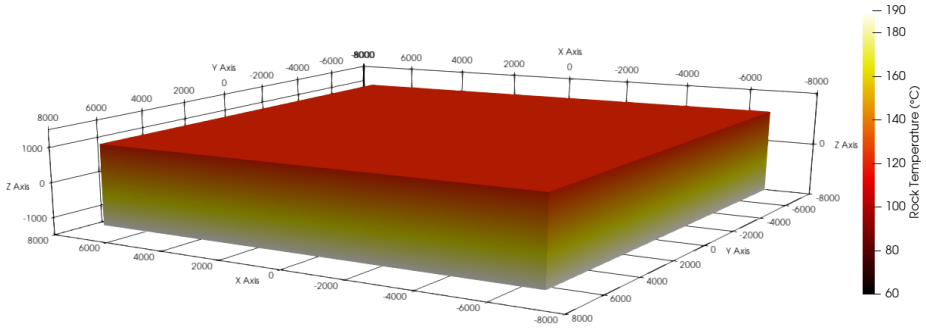

Figure 2: The homogeneous subsurface simulation domain initialized with the vertical geothermal gradient.

Table 1: OGS BHE_1P Simulation Parameters

Rock Parameters	Value	**Fluid Parameters**	Value
Rock Thermal Conductivity	3.35 W / (m · K)	Fluid Inlet Temperature	60 °C
Rock Density	2650 kg / m^3	Flow Rate (Loop)	0.0151 m^3 / s
Reservoir Porosity	0.07	Flow Rate (Radial Lateral)	0.00755 m^3 / s
Geothermal Gradient	30 °C / km	Pipe Wall Thickness	0.0001 m
Lateral Length	3500 m	Grout Thermal Conductivity	3.35 W / (m · K)
Lateral Borehole Diameter	0.216 m	Fluid Type	Water
Heat Flux	0.065 W / m^2	Reference Fluid Density (STP)	999.2 kg / m^3
Specific Heat Capacity	1047.2 J / (kg · K)	Specific Heat Capacity	4190 J / (kg · K)

3.2 Geometric Configurations Tested

To isolate the impact of radiator topology on thermal performance, we evaluated five distinct geometric configurations. To ensure an accurate comparison, the Total Borehole Heat Exchanger (BHE) length was conserved across the primary comparative scenarios. For example, the Reference Stacked Loop scenario comprises 6 loops ($L_{Total} \approx 37{,}165$m), while the equivalent TRS scenario with 2 opposing lateral arrays (TRS 2x6) comprises 12 laterals ($L_{Total} \approx 37{,}165$m).

Hydraulic parameters were similarly normalized to ensure thermodynamic parity. Since the TRS architecture utilizes double the number of laterals (12) compared to the Reference Loop (6) to achieve the same total drilled length, the mass flow rate per borehole was adjusted to maintain a constant Total System Flow Rate ($\dot{m}$) across all comparative simulations. Specifically, the Reference Loop scenarios were simulated with a flow rate of 15.1 kg/s per loop (Eavor Technologies Inc., 2020), while the TRS laterals used a flow rate of 7.55 kg/s per lateral. This ensures that both systems circulate the same aggregate volume of working fluid, isolating the heat extraction efficiency of the geometry itself.

Mesh refinement of 0.5m was applied at all convergence zones (hubs and heels) to resolve the acute thermal gradients caused by high pipe density, 10m near pipes to balance accuracy with speed, and 500m in the far field to avoid unproductive calculations on stagnant rock. Boundary conditions were standardized across all domains: a constant heat flux of 0.065 W/m^2 was applied to the bottom surface to represent crustal heat flow, while the top surface was held at a constant temperature to simulate surface radiation. The rock temperature was set so the bottom laterals were in 160°C rock.

3.2.1 Control and Baseline Scenarios

These configurations establish the thermal potential of the reservoir absent of complex interference effects. The controls are a single 3km horizontal BHE and a single 6.075 km loop (Figure 1), representing the maximum possible heat extraction per meter of drilled pipe (zero interference).

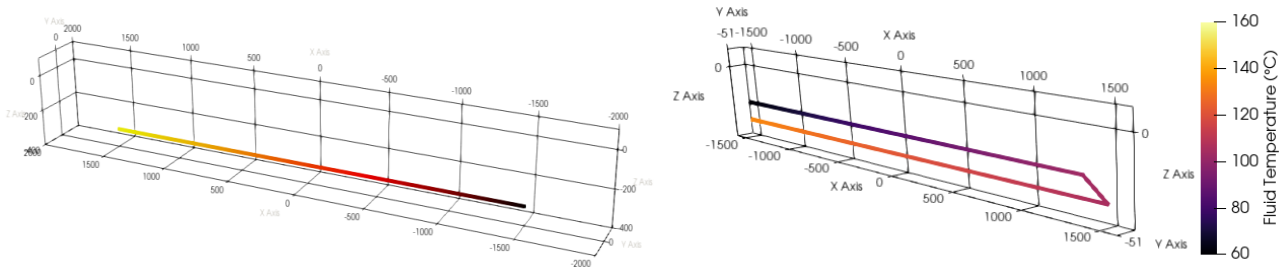

Figure 2: Control Scenarios - single 3km borehole (left) and a single 6.075km loop (right).

3.2.2 Baseline Reference Scenario

The baseline is a simplified radiator geometry representative of current state-of-the-art closed-loop commercial pilots (e.g., Geretsried). This configuration consists of 6 parallel loops arranged horizontally with uniform spacing, where in one loop, fluid flows from the inlet junction out across the top lateral, down to the bottom lateral, and back to the outlet junction.

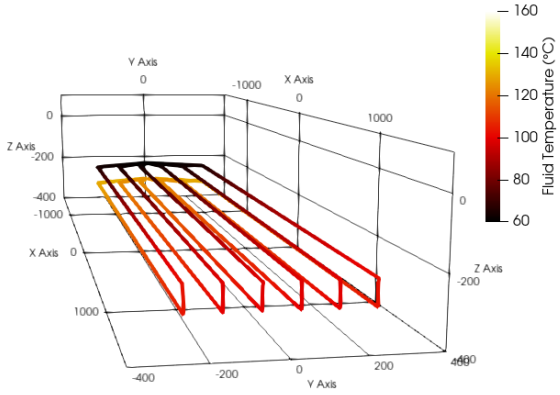

Figure 3: The reference vertically stacked radiator pattern to establish baseline thermal performance.

3.2.3 Telluric Radial System (TRS) Comparison Variations

The TRS 2x6 configuration (6 laterals going to each of 2 opposing outflows) is selected to evaluate the radial hub-and-spoke architecture, specifically testing the trade-offs between the high-density "pinch" at the central hub and the diverging flow in the far field, combined with the effects of 4 pinch points compared to 2 pinch points in the baseline. This configuration is tested once with all 12 laterals matching the depth of the bottom layer of the baseline configuration, and again with 6 laterals matching the depth of the top laterals of the baseline to match the total drilled distance at each depth.

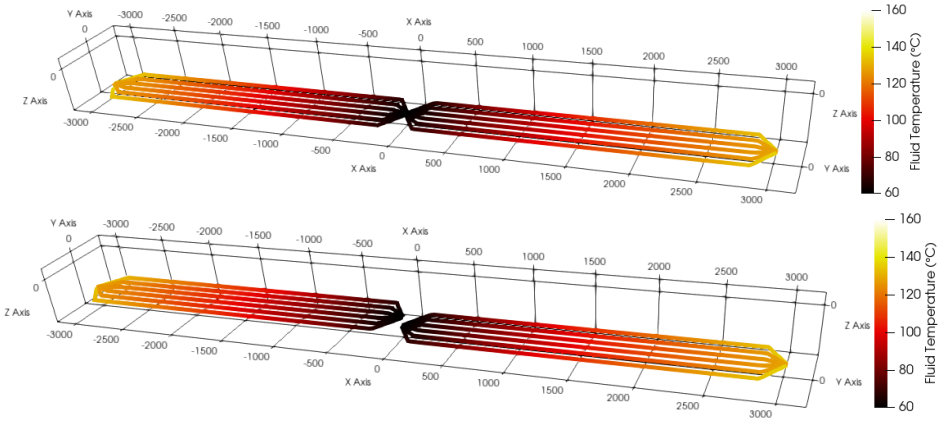

Figure 4: TRS Comparison Scenarios – TRS 2x6: 12 laterals at max depth (top) and TRS 2x6 Matched Depth: 12 laterals with 6 matching the depth of the top reference loop (bottom).

3.2.4 Sub-Study: Vertical Sensitivity (75m vs. 150m)

A critical variable in closed-loop performance is the vertical separation between the "Cold" injection horizon and the "Hot" production horizon (or the stacked laterals). To quantify this sensitivity, the Reference Stacked Loop and TRS 2x6 scenarios were simulated at two distinct vertical offsets, 75m and 150m, to isolate effects of vertical separation from horizontal topology.

3.2.5 Telluric Radial System (TRS) Phased Scaling Demonstrations

To visualize the thermal impact of incremental capacity expansion ("Phased Scaling"), two additional TRS configurations were modeled. These scenarios simulate the sequential activation of reservoir sectors, a unique capability of the radial architecture that allows for staged capital deployment on the same well. These scenarios use vertical offsets in addition to horizontal offsets between laterals, both representing a more realistic drilling configuration and highlighting the benefits of vertical staggering as opposed to vertical stacking. TRS Quad-Sparse: 3 laterals connecting to each of 4 outflows. This totals 12 3km laterals, 36km in total length without modeling the intersections. TRS Quad-Dense: this visualizes 6 laterals connecting to each of 4 outflows. This totals 24 3kms laterals, 72km in total length without modeling the intersections.

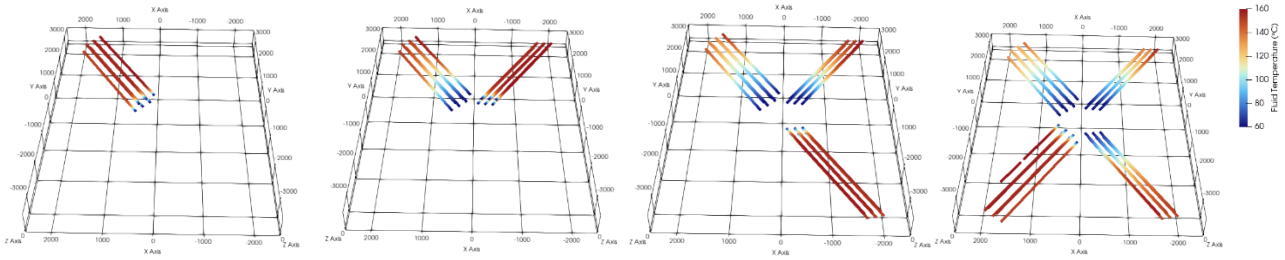

Figure 5: TRS Phased Scaling visualization with 6 laterals being added every year.

4. ANALYTICAL SYSTEM EVALUATION

While the Finite Element Analysis (Section 5) resolves the heat exchange within the reservoir, the net system performance depends on the coupled hydraulic behavior of the vertical wellbores, lateral arrays, and surface gathering network. We employ an analytical loop model to determine the net hydraulic power balance, explicitly accounting for the trade-off between buoyancy drive and frictional losses across the varying flow regimes of the hub-and-spoke topology.

4.1 Governing Equations

The system is modeled as a closed hydraulic circuit where the driving buoyancy pressure (ΔP_{buoy}) must overcome the cumulative frictional pressure losses (ΔP_{fric}) to sustain passive circulation at desired flow rates as a function of time t. The net system pressure (ΔP_{net}) determines the operational mode. If $\Delta P_{\mathrm{net}} > 0$, the system sustains passive thermosiphon flow. Otherwise, the deficit represents the parasitic pumping overhead.

$$\Delta P_{net}(t) = \Delta P_{buoy}(t) - \Delta P_{fric}(t)$$

4.1.1 Thermosiphon Drive (The Engine)

The buoyancy potential is derived from the cyclic integral of fluid density changes across the vertical extent of the closed-loop circuit (Oldenburg et al. 2016):

$$\Delta P_{buoy} = \oint \rho(P,T) \cdot g \cdot dz$$

where ΔP_{buoy} is the thermosiphon driving pressure, z is the vertical elevation coordinate, $\rho(P,T)$ is the fluid density as a function of pressure P and temperature T, and g is gravitational acceleration. While a fully realized field deployment would involve non-trivial deviated trajectories where every inclined section contributes to the net hydrostatic head, this study assumes a simplified orthogonal geometry (vertical shafts and horizontal laterals) to isolate the reservoir performance variables. Under this assumption, the net buoyancy drive reduces to the hydrostatic pressure differential between the centralized cold injection column and the distributed hot production columns.

$$\Delta P_{buoy} = \int_0^{z_{TD}} \left(\rho_{inj}(P,T_{in}) - \rho_{prod}(P,T_{out})\right) \cdot g \cdot dz$$

where ρ_{inj} and ρ_{prod} are the densities of the injection and production fluids respectively, and z_{TD} is the total depth of the wells.

4.1.2 Hydraulic Resistance (The Brake)

Frictional losses are calculated using the Darcy-Weisbach equation with the Haaland approximation (Haaland, 1983), summed across four distinct hydraulic domains: the Central Injector inj, the Lateral Array lat, the Satellite Outflows out, and the Surface Gathering Lines

$surf$. Crucially, the TRS architecture distributes the total mass flow $\dot{m}_{\text{total}}$ across N_{lat} laterals, and N_{out} outflow wells and surface pipes, significantly reducing velocity-dependent losses in those sections:

$$\Delta P_{fric} = \Delta P_{inj} + \Delta P_{lat} + \Delta P_{out} + \Delta P_{surf}$$

The injector carries full flow $\dot{m}_{total}$ and is modeled with a tapered profile where a large bore surface section transitions to standard casing at depth. Assuming equalized flow, the laterals each carry $\dot{m}_{\text{total}}$ / N, minimizing the friction penalty of the long horizontal sections. The outflows and surface pipes both carry $\dot{m}_{\text{total}}/\text{N}_{\text{out}}$ back to the central hub.

4.2 Sensitivity Variables

To validate if the "Quad-Dense" scaling scenario can achieve desired flow (181.2 kg/s) passively, we evaluate the hydraulic viability under two injector completion profiles: a standard taper including a 18-5/8" surface casing (17-1/2" internal diameter ID) at 2,000m depth tapering to 9-5/8" (8.5" ID), and a large-bore starting with a 20" surface casing (19-1/4" ID) to 2,000m depth tapering to a 13-3/8" (12-1/2" ID) to total depth. Outflow and surface pipes will use a 9-5/8" casing, and the lateral borehole diameter used is 8.5" in all scenarios.

Additionally, the impact of wellbore heat loss on the thermosiphon drive by varying the thermal insulation quality of the vertical injection, production, and return wells is quantified by testing three distinct effective thermal conductivity values (k_{eff}) for the wellbores. k_{eff} values of 0.05 W/mK represent pristine VIT, 0.5 W/mK represents degraded VIT, and 2.0 W/mK represents a standard non-insulated completion or catastrophic vacuum loss.

4.3 Computational Implementation & Thermal Sensitivity Methodology

To quantify the impact of infrastructure variables on system viability, a coupled thermal-hydraulic solver was developed in Python. This solver takes the transient reservoir outlet temperatures ($T_{res}(t)$) generated by the OGS finite element model and integrates the wellbore physics to determine the net thermosiphon pressure ($\Delta\text{P}_{\text{net}}$) at each time step.

4.3.1 Wellbore Heat Transmission Model

This study explicitly models the non-isothermal evolution of the working fluid as it traverses the vertical injection and production columns. As the fluid descends the injection well, it gains heat from the surrounding formation (reducing density and buoyancy drive). As fluid ascends the production well, it loses heat to the overburden and surface air.

To determine the temperature profile $T(z)$ along the vertical wellbores, we utilize the Ramey (1962) heat transmission model, which approximates the wellbore as a heat exchanger interacting with the linear geothermal gradient. The fluid temperature at depth z is calculated as an exponential relaxation toward the surrounding formation temperature $T_{earth}(z)$

$$T(z) = T_{earth}(z) - A\Gamma + \left(T_{in} - T_{surf} + A\Gamma\right) \cdot e^{-\frac{z}{A}}$$

where Γ is the thermal gradient, and A is the relaxation distance parameter (higher values indicate superior thermal retention), a function of the mass flow rate, fluid heat capacity c_p. The parameter A represents the ratio of thermal inertia to heat loss, defined as $A = \frac{\dot{m}c_p}{U}$, where $\dot{m}$ is the mass flow rate. The value of U is derived from the effective thermal conductivity k_{eff} sensitivity variable ($U \approx 2\pi k_{eff}$), allowing us to quantify the impact of VIT insulation quality on buoyancy drive.

assuming a standard logarithmic conduction profile through wellbore completions. This model is applied stepwise to both the injection leg (downward flow, heating) and the production leg (upward flow, cooling) to generate accurate density profiles for the buoyancy integration.

4.3.2 Environmental Boundary Conditions

The thermal exchange is governed by the following environmental parameters, representative of the Molasse Basin context, using a surface T_{surf} and ambient air temperature T_{air} of 10°C, and a total depth of 4,575m, in combination with the same values used previously for geothermal gradient and injection fluid properties.

4.3.3 Density & Friction Integration

The fluid density profile $\rho(\text{P},\text{T})$ is calculated using the IAPWS-97 standard formulation for industrial water properties (IAPWS 2012). The friction pressure drop is integrated stepwise across the varying wellbore geometries defined in Section 4.2. Specifically, the solver compares the hydraulic performance of the "Standard Taper" against the "Large-Bore" injector scenario by explicitly calculating the velocity-dependent friction losses in the upper (0 to 2,000m) and lower (2,000 to 4,575) sections. This allows for a direct evaluation of whether the reduced friction of the larger diameter profile effectively compensates for the increased thermal surface area and associated heat gain.

5. RESULTS AND DISCUSSION

5.1 Reservoir Thermal Performance

The finite element analysis reveals a distinct thermodynamic divergence between the parallel-stacked and radial topologies as the vertical spacing between stacked loop boreholes decreases.

5.1.1 Baseline vs. Radial Drawdown (Qualitative)

A single 3km lateral shows an outflow temperature of 126 °C at depth after 30 years, whereas the 6,075m out and back loop's outflow temperature was 122.4 °C. The reference stacked loop baseline laterals with 75m vertical and 100m horizontal separation exhibits a cold zone between its vertically stacked laterals. As illustrated in Figure 6, a horizontal slice of rock volume halfway between the upper and lower laterals is visibly colder after 5 years, continuing to cool significantly (~30°C over 30 years). With 150m vertical separation, the thermal drawdown at the halfway depth is significantly reduced (~10°C over 30 years).

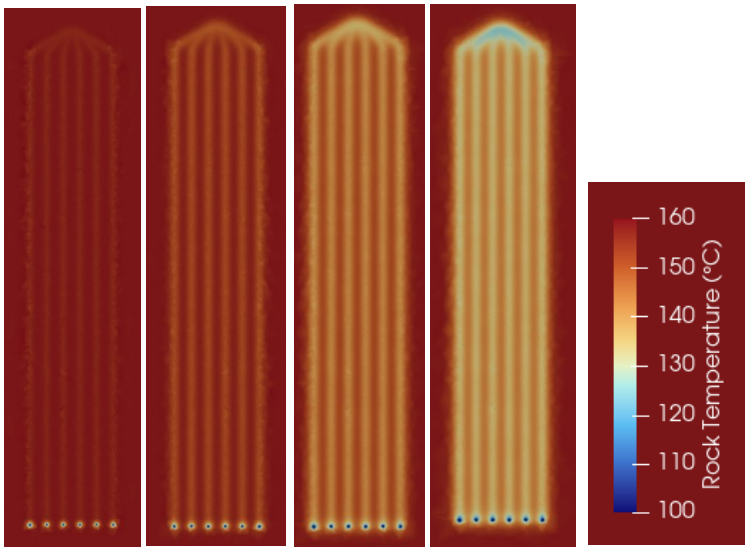

Figure 6: Thermal drawdown halfway between top and bottom lateral pairs with 100m horizontal spacing after 5, 10, 20, and 30 years (left to right).

In comparison, for the radial topology, while the thermal drawdown is also visible at the same depth after 5 years (37.5m above the lowest laterals), Figure 7 shows that heat is being extracted from a significantly wider reservoir volume. The radial divergence prevents the formation of a concentrated cold cores near hot pipe near the outflows, maintaining a higher average temperature in the inter-lateral rock matrix.

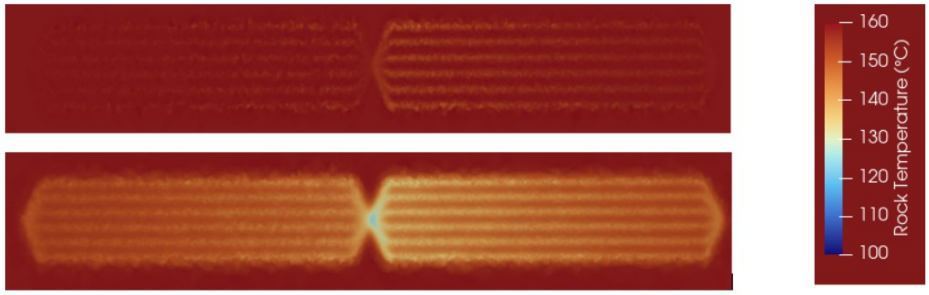

Figure 7: Thermal drawdown halfway between top and bottom lateral pairs with 100m horizontal spacing after 5 years (top) and 30 years (bottom). The left radiator is 75m higher than the right radiator, matching the depth of the reference.

5.1.2 Quantitative Comparison: Horizontal Spacing Sweep and Geometric Efficiency

The visual drawdown patterns translate directly to system performance. Figure 8 presents the aggregate thermal history of the Reference Stacked Loop versus the TRS 2x6 configuration. Both systems were normalized for total drilling length and total mass flow rate.

The Reference Stacked Loop (Blue) exhibits a steep initial decline, stabilizing at a lower outlet temperature due to the rapid depletion of the confined rock volume between the vertical legs. Conversely, the TRS 2x6 (Orange) maintains a flatter decline curve. Despite the high interference at the central "hub" (where 12 pipes converge), the diverging geometry ensures that fluid constantly moves into thermally un-depleted rock. By Year 30, the TRS average outlet temperature remains approximately 5°C higher than the equivalent length Reference Loop, showing that geometric divergence mitigates far-field thermal interference. For the 75m vertical separation scenarios, the horizontal separation between laterals increases, so does the difference between output temperatures.

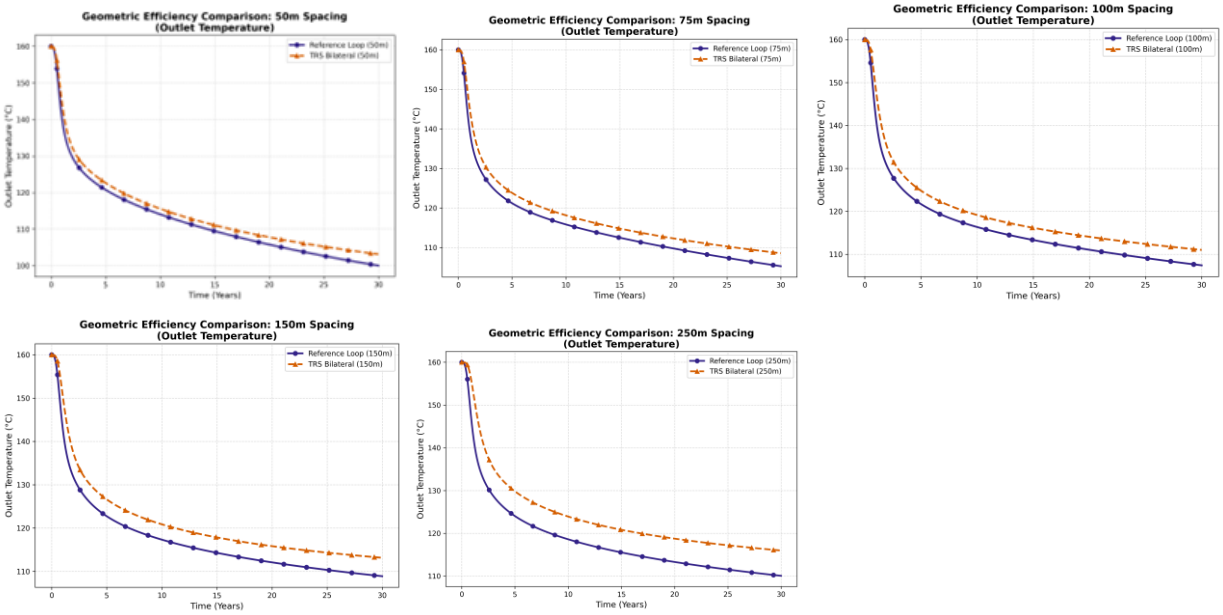

Figure 8: Horizontal lateral spacing sweep results highlight 5°C change in outflow temperatures over 30 years.

5.1.3 Vertical Sensitivity & Depth Constraints

Figure 4 compares the Reference Loop at vertical separation of 75m (standard) and 150m (optimized) against the matched depth TRS variant. In the matched depth case with 75m vertical separation between layers, TRS outflow temperatures are still 3°C higher than the reference loop. When the vertical separation increases to 150m, the temperature difference with the matched depth case is <1°C.

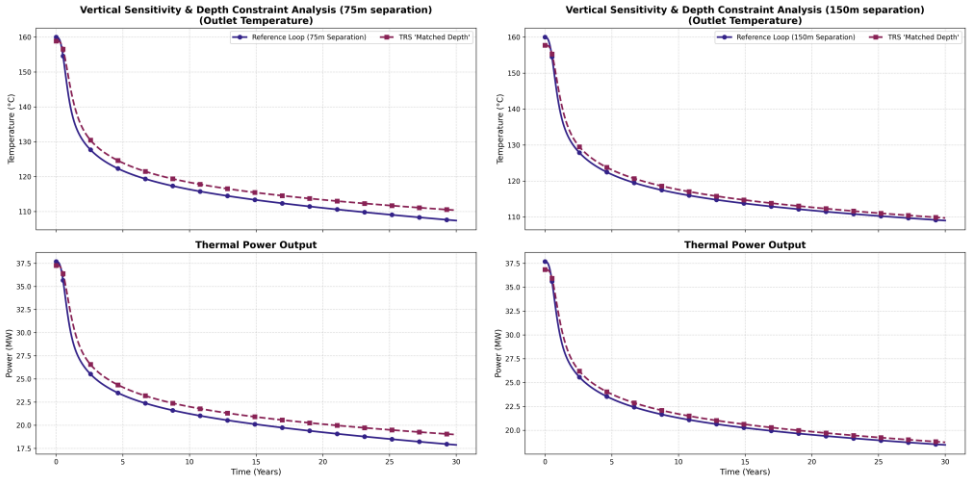

Figure 9: Impact of vertical spacing on radiator thermal drawdown. The radial topology competes effectively with multi-layer stacked designs without drilling deeper laterals

5.1.4 Phased Scaling & Interference

Figure 5 illustrates the thermal impact of incrementally adding new lateral groups with both horizontal and vertical offsets over time. Two configurations are shown, one with groups of 3 boreholes added every 6 months, and one with groups of 6 parallel boreholes added every year. Parallel laterals have uniform horizontal spacing and use a staggered vertical spacing of 60m across a 300m vertical section of rock. While doubling the number of parallel laterals in a single group increases power, it introduces a noticeable interference penalty, visible as

a steeper temperature decline in the "Dense" scenario. However, the system avoids thermal collapse, confirming that the radial geometry can support high-density development if the spacing at the central well remains sufficient.

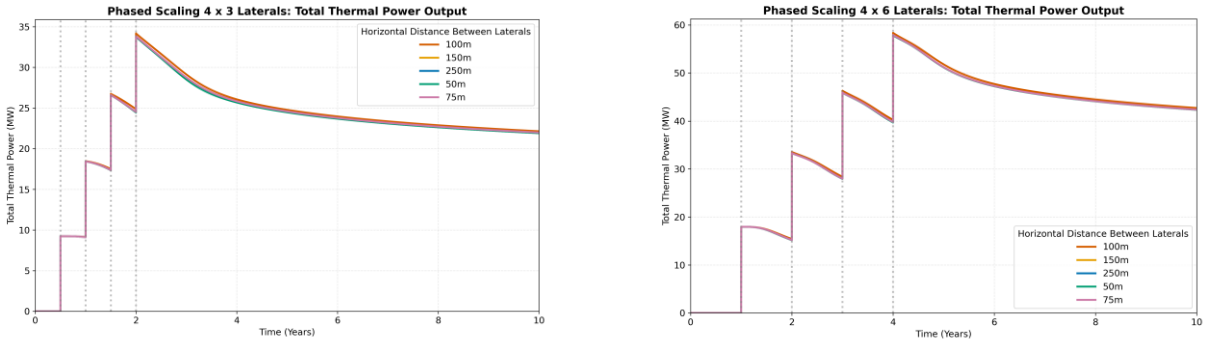

Figure 9: TRS Power vs. time graphs showing incremental increase in produced thermal power as laterals are added over time.

5.2 System Hydraulic Viability (Thermosiphon)

The analytical hydraulic model identifies the central injection well as the critical bottleneck for scaling to high-capacity ("Quad-Dense") flow rates (181.2 kg/s).

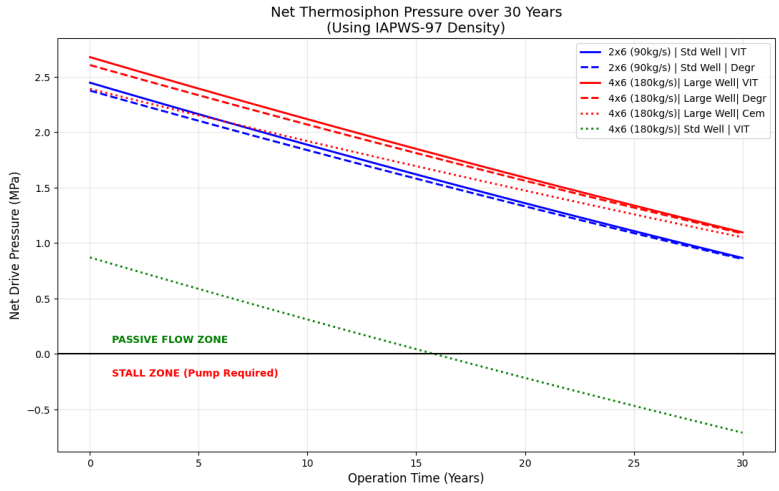

Figure 10: Temporal evolution of Net Thermosiphon Drive Pressure over the 30-year system life.

Results account for variable fluid density. The "Quad-Dense" scenario (4x6 laterals, Red Lines) maintains strong passive flow (>1.0 MPa) only when utilizing Large-Bore injector completions. Attempting to drive Quad-scale flow rates (181.2 kg/s) through standard completions (Green Dotted Line) results in excessive friction and system stall by Year 15. Note that the thermal retention benefit of VIT (Solid Lines) vs. Cemented completions (Dotted Lines) is secondary to hydraulic optimization at these high mass flow rates.

Consequently, these results confirm that for utility-scale deployments, increasing the casing diameter has a more significant effect than maximizing insulation values. The "Large-Bore" configuration decouples the system's thermal capacity from its hydraulic limitations, preserving a robust passive drive of >1.0 MPa throughout the 30-year lifecycle at 181.2 kg/s.

5.2.1 Alternative Working Fluids

While this study utilizes water as the baseline heat transport medium, utilizing alternative fluids with lower viscosity and higher thermal expansivity, such as supercritical carbon dioxide (sCO_2) would reduce the need for such large wellbore diameters. sCO_2 generates strong thermosiphon forces even in smaller pipes due to its density's high sensitivity to temperature (Adams et al. 2015). However, the implementation of non-aqueous fluids introduces significant engineering challenges, including geochemical instability, casing corrosion risks in the event of formation water ingress, and the need for specialized high-pressure surface handling equipment. Thus, water remains the baseline choice for immediate constructability, provided the wellbore geometry is optimized to the large-bore specifications described above.

5.3 Discussion and Future Research

5.3.1 Modeling Assumptions

To isolate the thermal performance of radial subsurface radiator topologies, this study employed a decoupled modeling approach, utilizing Finite Element Analysis and IAPWS-97 state equations, necessitating several simplifying assumptions. Firstly, we assumed efficient hydraulic connectivity between the vertical hub and horizontal laterals. In a physical deployment, connecting 12 or 24 laterals from multiple outflows to the single central hub presents engineering challenges. Making those connections at 4.5km+ depth starting multiple kilometers away on the surface, without intersecting any existing pipes is the most significant challenge due to MWD uncertainty scaling with depth and inclination. Net system efficiency must also account for surface thermal transmission lines, which may favor district heating applications where the load is distributed, rather than centralized power generation. Future work must utilize Computational Fluid Dynamics (CFD) to model the specific turbulence and pressure drops at these connection nodes.

5.3.2 System Cohesion

Future work will move beyond modelling the subsurface loop in isolation computationally. A fully coupled model is required to capture the feedback loop between surface turbine load, fluid cooling, and the resulting real-time fluctuations in thermosiphon drive. Drilling and node interception analyses based on errors of physically realized navigation devices should also be performed.

5.3.3 The Trade-off: Drilling Efficiency vs. Areal Density

A critical trade-off between radial and parallel designs identified in this study is the balance between thermal efficiency and subsurface footprint. The TRS architecture effectively trades drilling and completion complexity for the ability to deploy capital to the same well in phases and manage flows between laterals, and improved thermal performance of radiators. The techno-economic viability of this system hinges on the cost and reliability of installing high-temperature multilateral junctions, along with the complexities of ranging and localization, which currently represent the primary engineering barriers. Additionally, the TRS architecture achieves higher outlet temperatures and heat extraction rates per well by accessing a massive volume of rock via spoke-like laterals. However, the size of this radial zone inherently limits how tightly multiple systems can be packed in a given area. The TRS is therefore best utilized for environments where the thermal benefits of radial geometries outweigh the costs specific to the geometry, including a larger injection well, requiring a distributed network of hot insulated pipes on the surface, ranging technologies to guide multilateral intersections, and downhole isolation nodes to enable them while controlling flow across laterals of different lengths, depths, and geometries.

6. CONCLUSION

A radial topology extracts more heat per meter drilled from deep reservoirs compared to out-and-back designs with close-proximity laterals. By integrating Finite Element Analysis with a coupled wellbore model, we have demonstrated that the TRS architecture can provide a passive baseload power source, provided that specific geometric and engineering constraints are met.

Key findings: 1) Spacing is the thermal multiplier. The radial geometry outperforms out-and-back designs by minimizing thermal interference. Maximizing the horizontal spacing and carefully selecting vertical spacing between laterals is an effective lever for optimizing reservoir outlet temperatures. 2) Passive thermosiphon drive at 181.2 kg/s flow is viable but conditional on wellbore diameter and working fluid properties, with thermal resistivity of vertical wells having a less significant effect. Otherwise, standard deep geothermal completions would require parasitic pumping within 15 years. A large-bore injection profile would significantly reduce friction and maintain a net positive drive. 3) At high mass flow rates enabled by the topology, the TRS is resilient to wellbore heat loss and provides additional unique benefits like the ability to isolate laterals and stage risk and capital incrementally on the same well.

Ultimately, the TRS design proves that performance can be driven by controllable geometric parameters rather than reservoir permeability, providing well construction and intersection engineering challenges to achieve greater thermodynamic efficiency and asset scalability.

REFERENCES

Adams, B.M., Kuehn, T.H., Bielicki, J.M., and Saar, M.O. (2015). A comparison of CO2 and water as working fluids for a closed-loop geothermal system. Journal of Cleaner Production, 94, 264-275.

Beckers, K., and Johnston, H.: Techno-Economic Performance of Eavor-Loop 2.0, Proceedings, 47th Workshop on Geothermal Reservoir Engineering, Stanford University, Stanford, CA (2022).

Bilke, L., Flemisch, B., Kalbacher, T., Kolditz, O., Helmig, R., and Nagel, T.: Development of Open-Source Porous Media Simulators: Principles and Experiences, Transport in Porous Media, 130, (2019), 337-361.

Eavor Technologies Inc.: Technological Innovations in Deep Geothermal Energy, Written Evidence, Environmental Audit Committee, House of Commons, UK Parliament (2020).

Haaland, S.E.: Simple and Explicit Formulas for the Friction Factor in Turbulent Pipe Flow, Journal of Fluids Engineering, 105(1), (1983), 89-90.

Halliburton: Rotating Magnet Ranging System (RMRS) Technical Data Sheet, (2024). Available at: https://www.halliburton.com

IAPWS: Revised Release on the IAPWS Industrial Formulation 1997 for the Thermodynamic Properties of Water and Steam, The International Association for the Properties of Water and Steam, Lucerne, Switzerland (2012).

Kelly, J.J., and McDermott, C.I.: Numerical Modelling of a Deep Closed-Loop Geothermal System: Evaluating the Eavor-Loop, AIMS Geosciences, 8(2), (2022), 175-212.

Oldenburg, C.M., Pan, L., Muir, M.P., Eastman, A.D., and Higgins, B.S.: Numerical Simulation of Critical Factors Controlling Heat Extraction from Geothermal Systems Using a Closed-Loop Heat Exchange Method, Proceedings, 41st Workshop on Geothermal Reservoir Engineering, Stanford University, Stanford, CA (2016).

Ramey, H.J.: Wellbore Heat Transmission, Journal of Petroleum Technology, 14(04), (1962), 427-435.

Richter, A.: Eavor reports drilling to 7000m measured depth at Geretsried project, Germany, ThinkGeoEnergy (2024).

Schlumberger: TAML Level 5 Multilateral Junction Technology, Schlumberger Technical Documentation (2023).

Scientific Drilling: BlackStream AMR - Active Magnetic Ranging Tool Specification Sheet, Scientific Drilling International (2024).

Tester, J.W., et al.: The Future of Geothermal Energy: Impact of Enhanced Geothermal Systems (EGS) on the United States in the 21st Century, Massachusetts Institute of Technology, Cambridge, MA (2006).

Toews, M., Brown, C., Holmes, M., and Zatonski, V.: Case Study of a Multilateral Closed-Loop Geothermal System, Proceedings, 45th Workshop on Geothermal Reservoir Engineering, Stanford University, Stanford, CA (2020).